Extended triaxial projected shell model approach for odd-neutron nuclei

S. Jehangir [1,*] Nazira Nazir [2] G. H. Bhat [3,4,†] J. A. Sheikh [2,‡] N. Rather [1] S. Chakraborty [5] and R. Palit [6]

[1]*Department of Physics, Islamic University of Science and Technology, Jammu and Kashmir 192 122, India*
[2]*Department of Physics, University of Kashmir, Hazratbal, Srinagar 190 006, India*
[3]*Department of Physics, S.P. College, Srinagar, Jammu and Kashmir 190 001, India*
[4]*Cluster University Srinagar, Jammu and Kashmir, Srinagar, Goji Bagh 190 008, India*
[5]*Physics Group, Variable Energy Cyclotron Centre, Kolkata 700 064, India*
[6]*Department of Nuclear and Atomic Physics, Tata Institute of Fundamental Research, Mumbai 400 005, India*

(Received 23 March 2022; accepted 21 April 2022; published 13 May 2022)

In an effort to elucidate the rich band structures observed in odd-neutron systems, the triaxial projected shell model approach is extended to include three-quasineutron and five-quasiparticle configurations. This extension makes it possible to investigate the high-spin states up to and including the second band crossing. Detailed investigation has been performed for odd-mass Xe isotopes with the extended basis, and it is shown that the character of the band crossing along the yrast line changes with shell filling of the $1h_{11/2}$ orbital. Further, it is observed that the three-quasiparticle state that crosses the ground-state configuration, leading to the normal band crossing phenomenon along the yrast line, first crosses the γ band based on the ground-state configuration at an earlier spin value. This crossing feature explains the occurrence of the signature inversion observed in the γ bands for some of the studied isotopes.

DOI: 10.1103/PhysRevC.105.054310

I. INTRODUCTION

In recent years, some major advancements in spectroscopic techniques have made it feasible to populate the high-spin band structures in atomic nuclei to the extremes of angular-momentum, excitation energy, and isospin [1–18]. In some nuclei, the high-spin states have been studied up to angular momentum $I \approx 60\hbar$, and as many as 20 sidebands have been identified [9–12,14]. The observation of these rich band structures poses a tremendous challenge to theoretical models to elucidate the properties of these structures. During the last several decades, the standard approach to describe the high-spin properties of deformed nuclei has been the cranked shell model (CSM) based on a modified harmonic oscillator [19,20] or Woods-Saxon potential [21]. Although this approach has provided some new insights into the structure of the high-spin states, it is known to have limited applicability. For instance, it is suited only for rotating systems, and the study of vibrational modes is beyond the scope of the basic CSM approach. Further, the CSM wave functions do not have well defined value of the angular momentum, and the evaluation of the transition probabilities using this approach becomes questionable [22].

The spherical shell model (SSM) approach has made great strides in recent years to explore the medium and heavier mass regions, and it has become possible to investigate the properties of nuclei in the mass region, $A \approx 120$–130 [23–30]. However, in order to study the high-spin band structures, it is essential to include, at least, the configuration space of two oscillator shells, which seems to be impossible with the existing computational facilities. The modern mean-field approaches based on Skyrme, Gogny, and relativistic density functionals, on the other hand, reproduce the known binding energies of nuclei all across the Segrè chart with a remarkable accuracy [31–36]. The problem with these approaches is that they are mostly limited to investigate the ground-state properties, as beyond-mean-field extensions using the projection methods lead to singularities [37–40], and further one encounters the conceptual problem of how to treat the density-dependent terms in the functionals of these approaches. In recent years, alternative approaches have been developed to map the energy surfaces obtained from the density functional onto Bohr [41–43] and interacting boson model (IBM) [44,45] Hamiltonians, and fit the parameters of these phenomenological approaches. These model Hamiltonians are then solved using the standard techniques to obtain the energies and electromagnetic properties of the nuclear systems. However, these alternative approaches are restricted, at the moment, to investigating ground-state band structures only.

In recent years, the triaxial projected shell model (TPSM) approach has been demonstrated to provide a unified description of the high-spin band structures of rotational and transitional nuclei with remarkable accuracy [56–58]. The advantage of this model is that basis space is composed of angular-momentum projected multiquasiparticle states which allows one to investigate the band structures up to quite high spin. The basic tenet of the TPSM approach is quite similar to that of the SSM approach with the only exception that

*sheikhahmad.phy@gmail.com
†gwhr.bhat@gmail.com
‡sjaphysics@gmail.com

TABLE I. Axial and triaxial quadrupole deformation parameters ε and ε' employed in the TPSM calculation.

	^{117}Xe	^{119}Xe	^{121}Xe	^{123}Xe	^{125}Xe	^{127}Xe	^{129}Xe	^{131}Xe
ε	0.234	0.227	0.209	0.220	0.180	0.150	0.150	0.160
ε'	0.110	0.100	0.100	0.105	0.090	0.100	0.095	0.090
γ	25	24	24	24	27	33	32	29

deformed bases are employed as compared to the spherical states. The deformed states form the optimum basis to investigate the properties of deformed nuclei.

In the earlier version of the TPSM approach, the basis space was quite limited, and it was not possible to investigate the high-spin states [59–65]. For odd-neutron systems, the basis space was one-neutron and one-neutron coupled to two-proton states. In the present work, we have expanded the basis space to include three-neutron and three-neutron coupled to two-proton configurations. This extension makes it feasible to investigate the odd-neutron systems up to quite high angular momentum and, as a first major application of this development, the high-spin band structures for odd-neutron $^{117-131}$Xe have been investigated in the present work. The present work is an ongoing effort of our group to extend the TPSM approach, and in our recent publications we have expanded the basis space of even-even [66], odd-odd [67], and odd-proton [68] systems. We would like to mention that in a parallel effort the axial version of the TPSM approach has also been generalized to multiquasiparticle states [69–72]. Further, beyond-mean-field density functional approaches employing angular-momentum and particle-number projection techniques have also been developed for the description of odd-mass nuclei [73,74].

The band structures in odd-mass Xe isotopes have been extensively investigated using state-of-the-art experimental techniques [10,49,75]. In some of these studies, the high-spin states have been populated up to spin $I \approx 55\hbar$, and also several sidebands have been identified [8,10]. The major problem is how to characterize the intrinsic configurations of the observed band structures as single-particle and collective degrees of freedom are interwoven in odd-mass systems. The extended TPSM approach developed in the present work

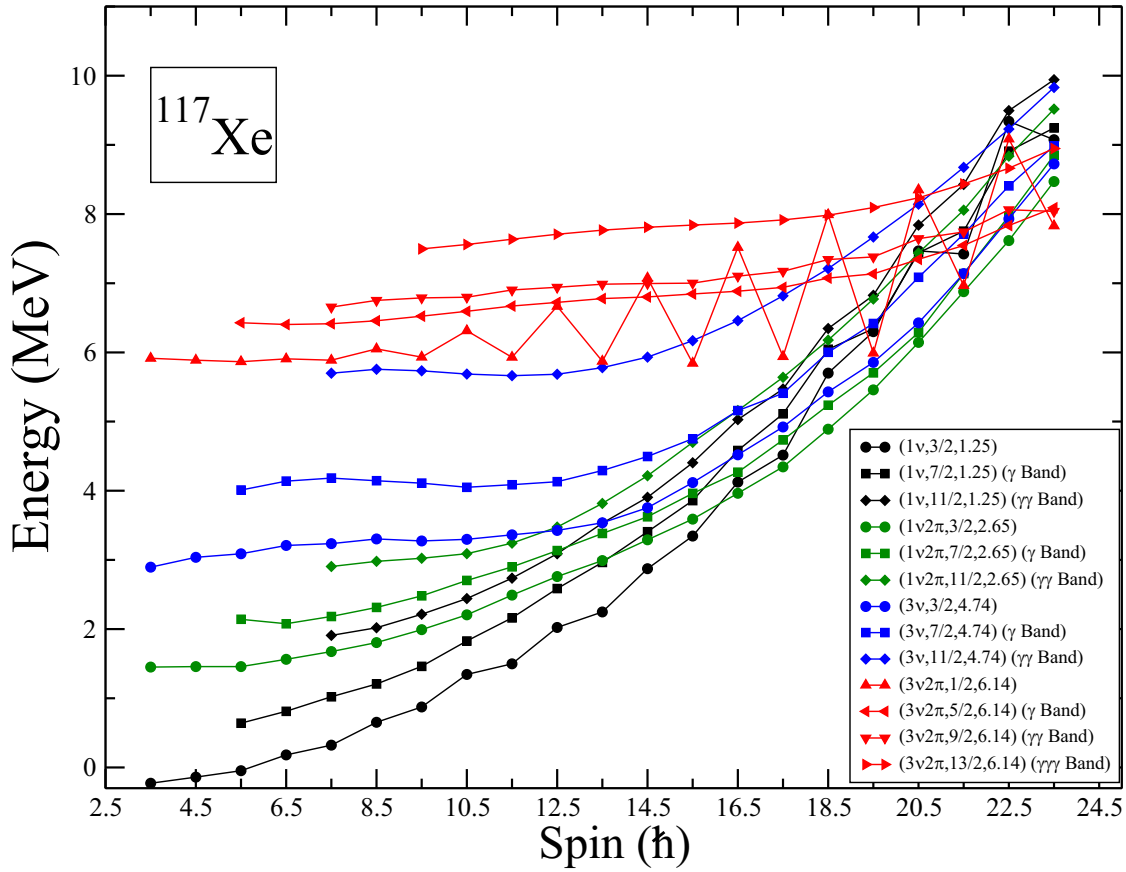

FIG. 1. Angular-momentum projected energies are shown before diagonalization of the shell model Hamiltonian for ^{117}Xe. The bands are labeled by three quantities: group structure, K quantum number, and energy of the quasiparticle state. For instance, $(1\nu, 3/2, 1.25)$ designates a one-quasineutron state having intrinsic energy of 1.25 MeV and $K = 3/2$. It is interesting to note that, apart from the normal band crossing at $I = 33/2$ between the three-quasiparticle configuration having energy of 2.65 MeV and $K = 3/2$ with the ground state band, the γ band built on the three-quasiparticle state having $K = 7/2$ also crosses the γ band based on the ground state at the same angular momentum. Further, the three-quasiparticle configuration first crosses the γ band around $I = 14$ before it crosses the ground state band. This crossing leads to the signature inversion phenomenon in the γ band.

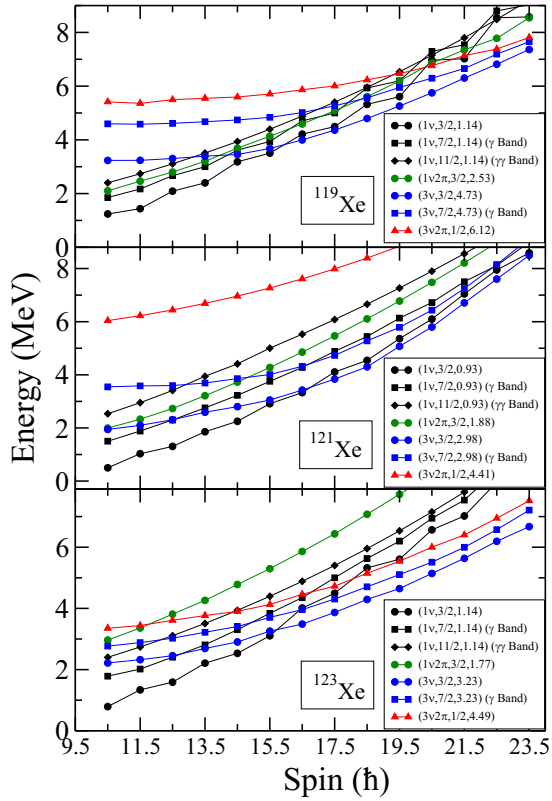

FIG. 2. Segments of the band diagrams for odd-neutron $^{119-123}$Xe isotopes. The bands are labeled as in Fig. 1.

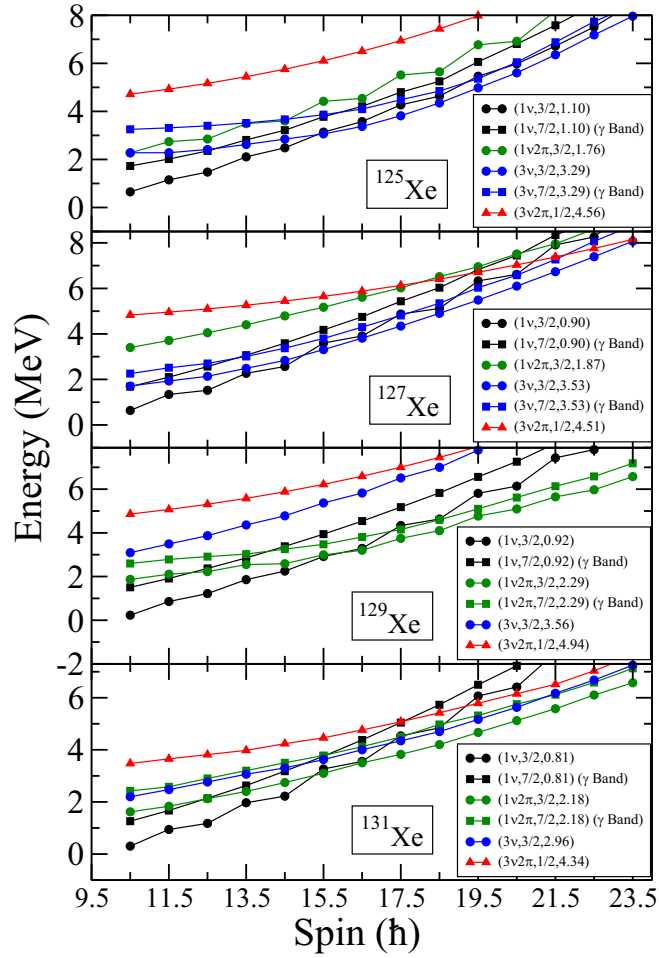

FIG. 3. Segments of the band diagrams for odd-neutron $^{125-131}$Xe isotopes. The bands are labeled as in Fig. 1.

provides a unified description of the single-particle and collective modes. It will be established in the present study that some excited bands observed in these nuclei are γ bands built on quasiparticle states. The observation of the signature inversion in the γ bands in some of the studied nuclei will also be addressed in the present work.

Further, it has been observed in the odd-neutron Xe isotopes that the character of the band crossing changes from proton to neutron with increasing mass number [10,49,75,76]. Because in the extended model space both proton and neutron quasiparticle configurations are included, it is possible to investigate the interplay between neutron and proton alignments. This interplay between different quasiparticle configurations shall be studied in detail in the present work. The paper is organised in the following manner. In the next section, the extended TPSM approach is briefly presented. In Sec. III, TPSM results obtained for odd-mass Xe isotopes are compared with the experimental data, wherever available. Finally, the results obtained in the present work are summarized and concluded in Sce. IV.

II. EXTENDED TRIAXIAL PROJECTED SHELL MODEL APPROACH

To provide a microscopic description of collective and multiquasiparticle excitations in odd-neutron systems, the TPSM approach has been extended by including three- and five-quasiparticle basis states. Odd-neutron systems have been studied earlier using the TPSM approach with the restricted model space of one-neutron and one-neutron coupled to two-proton quasiparticle states. However, in order to investigate the high-spin data, which is now available for many odd-neutron systems, neutron aligning configurations are needed, in addition to the proton aligning states. In the present work, the extended basis space has been implemented, and the complete basis space in the generalised approach is given by:

$$\begin{aligned} &\hat{P}^I_{MK}\, a^\dagger_{\nu_1}|\Phi\rangle, \\ &\hat{P}^I_{MK}\, a^\dagger_{\nu_1} a^\dagger_{\pi_2} a^\dagger_{\pi_3}|\Phi\rangle, \\ &\hat{P}^I_{MK}\, a^\dagger_{\nu_1} a^\dagger_{\nu_2} a^\dagger_{\nu_3}|\Phi\rangle, \\ &\hat{P}^I_{MK}\, a^\dagger_{\nu_1} a^\dagger_{\nu_2} a^\dagger_{\nu_3} a^\dagger_{\pi_1} a^\dagger_{\pi_2}|\Phi\rangle, \end{aligned} \tag{1}$$

where $|\Phi\rangle$ is the triaxially deformed quasiparticle vacuum state. $a^\dagger_{\nu_i}, a^\dagger_{\pi_i}$ are the quasiparticle creation operators with the index ν_i (π_i) denoting the neutron (proton) triaxial Nilsson states of the chosen configuration space. P^I_{MK} is the three-dimensional angular-momentum-projection operator given by [22]

$$\hat{P}^I_{MK} = \frac{2I+1}{8\pi^2}\int d\Omega\, D^I_{MK}(\Omega)\,\hat{R}(\Omega), \tag{2}$$

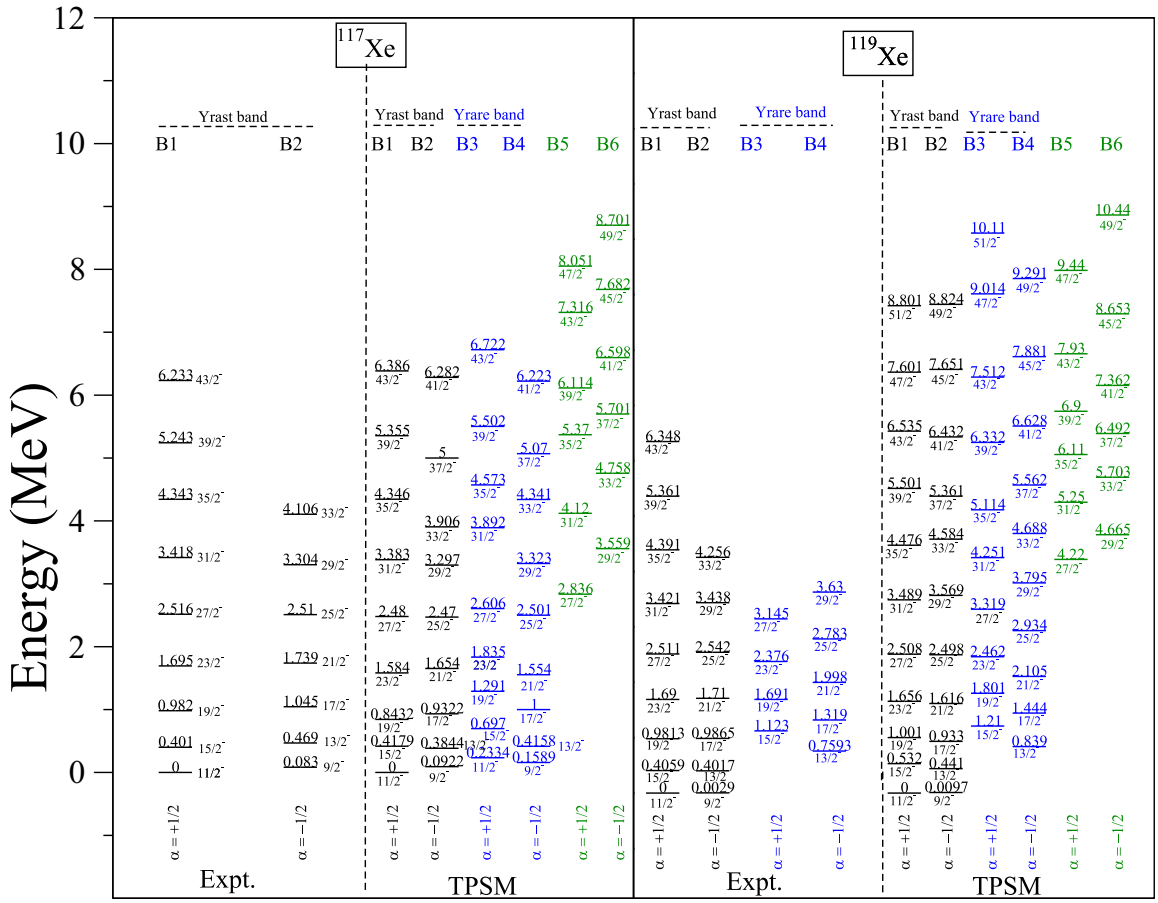

FIG. 4. TPSM energies for the lowest bands after configuration mixing are plotted along with the available experimental data for ^{117,119}Xe isotopes. Data were taken from [46,47].

with the rotation operator

$$\hat{R}(\Omega) = e^{-i\alpha\hat{J}_z} e^{-i\beta\hat{J}_y} e^{-i\gamma\hat{J}_z}. \tag{3}$$

Here, Ω represents the set of Euler angles ($\alpha, \gamma = [0, 2\pi]$, $\beta = [0, \pi]$) and $\hat{J}$'s are the angular-momentum operators.

The constructed projected basis of Eq. (1) is then used to diagonalize the shell model Hamiltonian. In this sense, the present approach is analogous to the SSM approach with the difference that the projected deformed basis is employed as compared to the spherical basis in the SSM approach. In the present work, the shell model Hamiltonian consists of a sum of quadrupole-quadrupole, monopole pairing, and quadrupole pairing interaction terms. These terms describe the principle components of the nuclear potential [77,78]. The Hamiltonian is given by

$$\hat{H} = \hat{H}_0 - \frac{1}{2}\chi \sum_{\mu} \hat{Q}^{\dagger}_{\mu}\hat{Q}_{\mu} - G_M \hat{P}^{\dagger}\hat{P} - G_Q \sum_{\mu} \hat{P}^{\dagger}_{\mu}\hat{P}_{\mu}. \tag{4}$$

In the above equation, $\hat{H}_0$ is the spherical single-particle part of the Nilsson potential [79]. As a consequence of the self-consistent HFB condition, the QQ-force strength, χ, in Eq. (4) is related to the quadrupole deformation ε. The monopole pairing strength G_M (in MeV) is of the standard form

$$G_M = \frac{G_1 \mp G_2 \frac{N-Z}{A}}{A}, \tag{5}$$

where the minus sign applies to neutrons and the plus sign applies to protons. In the present work, G_1 and G_2 are fixed such that the calculated gap parameters approximately reproduce the experimental odd-even mass differences in the mass region under investigation. The single-particle space employed in the present calculation is three major oscillator shells ($N = 3, 4, 5$) for both neutrons and protons. The strength G_Q for the quadrupole pairing force is fixed as 0.16 times the G_M strength. These interaction strengths are consistent with those used earlier in the TPSM calculations [61,64,80].

To diagonalize the shell model Hamiltonian, Eq. (4) in the angular-momentum projected basis, the Hill-Wheeler approach is followed [80]. The generalized eigenvalue equation is given by

$$\sum_{\kappa' K'} \left\{ \mathcal{H}^{I}_{\kappa K \kappa' K'} - E \mathcal{N}^{I}_{\kappa K \kappa' K'} \right\} f^{\sigma I}_{\kappa' K'} = 0, \tag{6}$$

where the Hamiltonian and norm kernels are given by

$$\mathcal{H}^{I}_{\kappa K \kappa' K'} = \langle \Phi_{\kappa} | \hat{H} \hat{P}^{I}_{K K'} | \Phi_{\kappa'} \rangle,$$
$$\mathcal{N}^{I}_{\kappa K \kappa' K'} = \langle \Phi_{\kappa} | \hat{P}^{I}_{K K'} | \Phi_{\kappa'} \rangle.$$

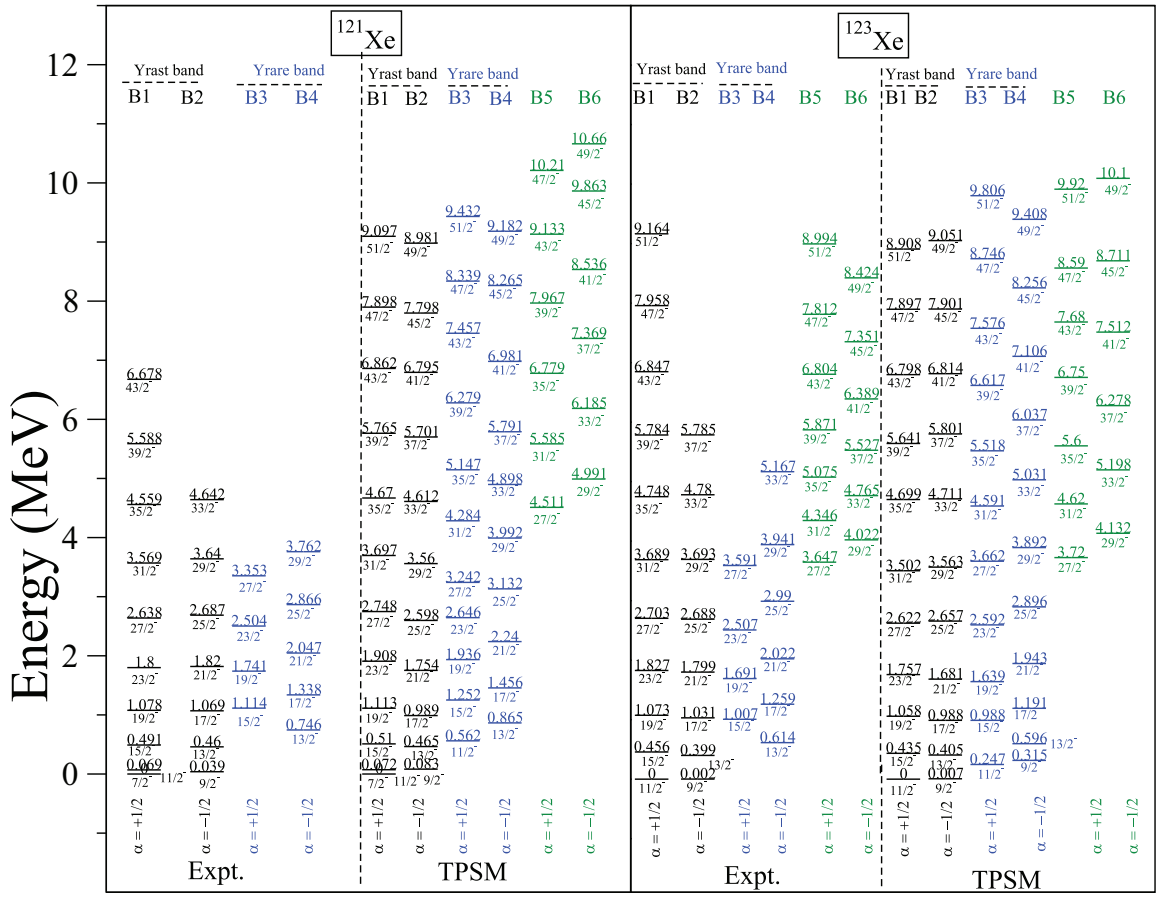

FIG. 5. TPSM energies for the lowest bands after configuration mixing are plotted along with the available experimental data for ^{121,123}Xe isotopes. Data were taken from [8,48].

The Hill-Wheeler wave function is given by

$$\psi^{\sigma}_{IM} = \sum_{\kappa,K} f^{\sigma I}_{\kappa K}\, \hat{P}^{I}_{MK}|\Phi_{\kappa}\rangle. \tag{7}$$

where $f^{\sigma I}_{\kappa K}$ are the variational coefficients and index κ designates the basis states of Eq. (1). The wave function is then used to evaluate the electromagnetic transition probabilities. The reduced electric transition probabilities B(EL) from an initial state (σ_i, I_i) to a final state (σ_f, I_f) are given by [58]

$$B(\mathrm{EL}, I_i \to I_f) = \frac{1}{2I_i+1}|\langle\psi^{\sigma_f I_f}||\hat{Q}_L||\psi^{\sigma_i I_i}\rangle|^2, \tag{8}$$

and the reduced matrix element can be expressed as

$$\begin{aligned}
&\langle\psi^{\sigma_f I_f}||\hat{Q}_L||\psi^{\sigma_i I_i}\rangle \\
&= \sum_{\kappa_i,\kappa_f,K_i,K_f} f^{\sigma_i I_i}_{\kappa_i K_i} f^{\sigma_f I_f}_{\kappa_f K_f} \sum_{M_i,M_f,M} (-)^{I_f - M_f} \\
&\quad\times \begin{pmatrix} I_f & L & I_i \\ -M_f & M & M_i \end{pmatrix} \langle\Phi|\hat{P}^{I_f}_{K_f M_f}\hat{Q}_{LM}\hat{P}^{I_i}_{K_i M_i}|\Phi\rangle \\
&= 2\sum_{\kappa_i,\kappa_f,K_i,K_f} f^{\sigma_i I_i}_{\kappa_i K_i} f^{\sigma_f I_f}_{\kappa_f K_f} \\
&\quad\times \sum_{M',M''} (-)^{I_f - K_f}(2I_f+1)^{-1} \begin{pmatrix} I_f & L & I_i \\ -K_f & M' & M'' \end{pmatrix} \\
&\quad\times \int d\Omega\, D^{I_i}_{M''K_i}(\Omega)\langle\Phi_{\kappa_f}|\hat{O}_{LM'}\hat{R}(\Omega)|\Phi_{\kappa_i}\rangle.
\end{aligned}$$

In the present work, we have evaluated the transition quadrupole moment, $Q_t(I)$, which is related to $B(E2)$ transition probability through

$$Q_t(I) = \sqrt{\frac{16\pi}{5}}\frac{\sqrt{B(E2, I \to I-2)}}{\langle I, K, 2, 0|I-2, K\rangle}. \tag{9}$$

In the numerical calculations, we have used the standard effective charges of $1.5e$ for protons and $0.5e$ for neutrons [80,81].

III. RESULTS AND DISCUSSION

TPSM calculations have been performed for eight odd-mass $^{117-131}$Xe isotopes using the axial and nonaxial deformations listed in Table I. These deformation values have been adopted from the earlier studies performed for these nuclei [10,46–49,51,52,75]. The angular momentum projected energies for the configurations in the vicinity of the Fermi surface are depicted in Figs. 1–3 for the studied isotopes. These plots, referred to as the band diagrams, provide important information on the intrinsic structures of the observed band structures, which in turn sheds light on the nature of band crossings. For ^{117}Xe, the projected energies from the lowest $I = 7/2$ to $47/2$ are depicted in Fig. 1. These diagrams are similar for all other studied Xe isotopes and only the interesting band crossing

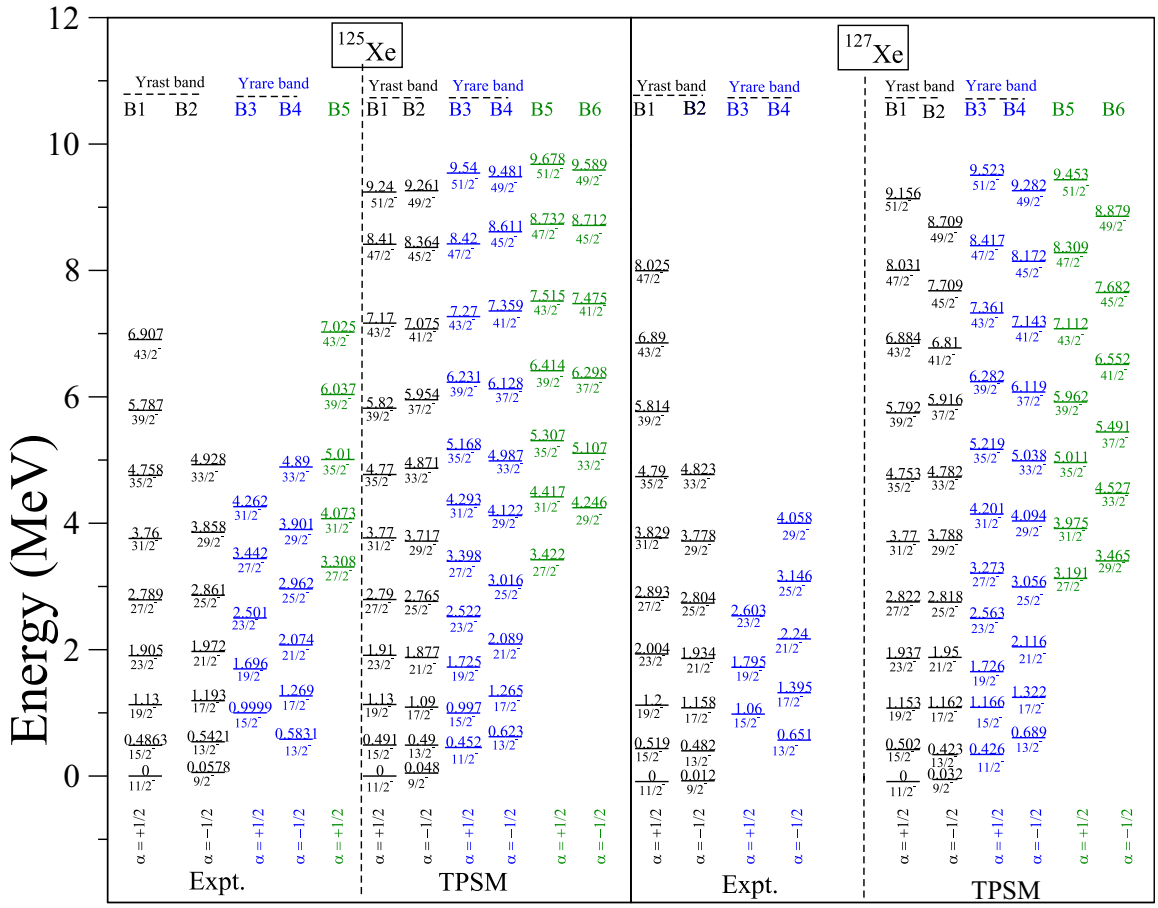

FIG. 6. TPSM energies for the lowest bands after configuration mixing are plotted along with the available experimental data for ^{125,127}Xe isotopes. Data were taken from[10,49,50].

portions of the diagrams are shown in Figs. 2 and 3 since the crossing features vary from isotope to isotope.

The ground-state band for ^{117}Xe is the projected band from the one-quasineutron configuration having $K = 3/2$ and intrinsic energy of 1.25 MeV. The projection from this triaxial intrinsic state also leads to several other band structures with $K = 7/2$ and $11/2$, which are so called γ and $\gamma\gamma$ bands built on the $K = 3/2$ state. The bandheads of these bands are located at excitation energies of 1.01 and 2.10 MeV, respectively. In recent years, several excited bands have been observed in Xe isotopes, and some of these bands have been conjectured to be the γ bands. It is one of the objectives of the present work to investigate these structures as candidate γ bands in odd-mass Xe-isotopes.

It is observed from Fig. 1 that the three-quasiparticle band with $K = 3/2$ configuration crosses the ground-state band at $I = 33/2$. This crossing of the configuration having one neutron coupled to two protons will correspond to the first band crossing observed for this system. It is quite interesting to note that $K = 7/2$, which is the γ band based on the three -quasiparticle state, also crosses the normal γ band built on the ground-state band. This is expected since γ bands are projected from the same intrinsic state as that of the parent state, but with a different value of K quantum number. Further, this band also crosses the ground-state band at a slightly higher angular momentum, and it is therefore predicted that at high-spin two parallel band structures should be observed, one corresponding to the normal one-neutron plus two-proton configuration and the other to the γ band based on it.

The segments of the band diagrams for other Xe isotopes that include only the band crossing regions are displayed in Figs. 2 and 3. For ^{119}Xe, the band crossing noted at $I = 33/2$ is due to alignment of neutrons rather than that of protons as for ^{117}Xe. For ^{121,123,125,127}Xe isotopes, the first crossing is again due to neutrons; however, for ^{129,131}Xe isotopes the alignment is due to protons as for the lighter isotope of ^{117}Xe. In most of the isotopes, it is noted that three-quasiparticle state having $K = 3/2$ and the γ band built on it almost simultaneously cross the ground-state band. This has been also found in several even-even systems in this region [82–84].

High-spin states in odd-neutron Xe-isotopes have been investigated by various experimental groups [10,46,47,49,51,52,75], and in some nuclei sidebands apart from the yrast states have been populated up to quite high angular momentum. In Figs. 4–7, the calculated band structures obtained after diagonalization of the shell model Hamiltonian are compared with the observed energies. TPSM band structures are plotted for the yrast, yrare, and also for the three-quasiparticle excited band, as in some of the studied nuclei excited bands have been observed. The purpose here is

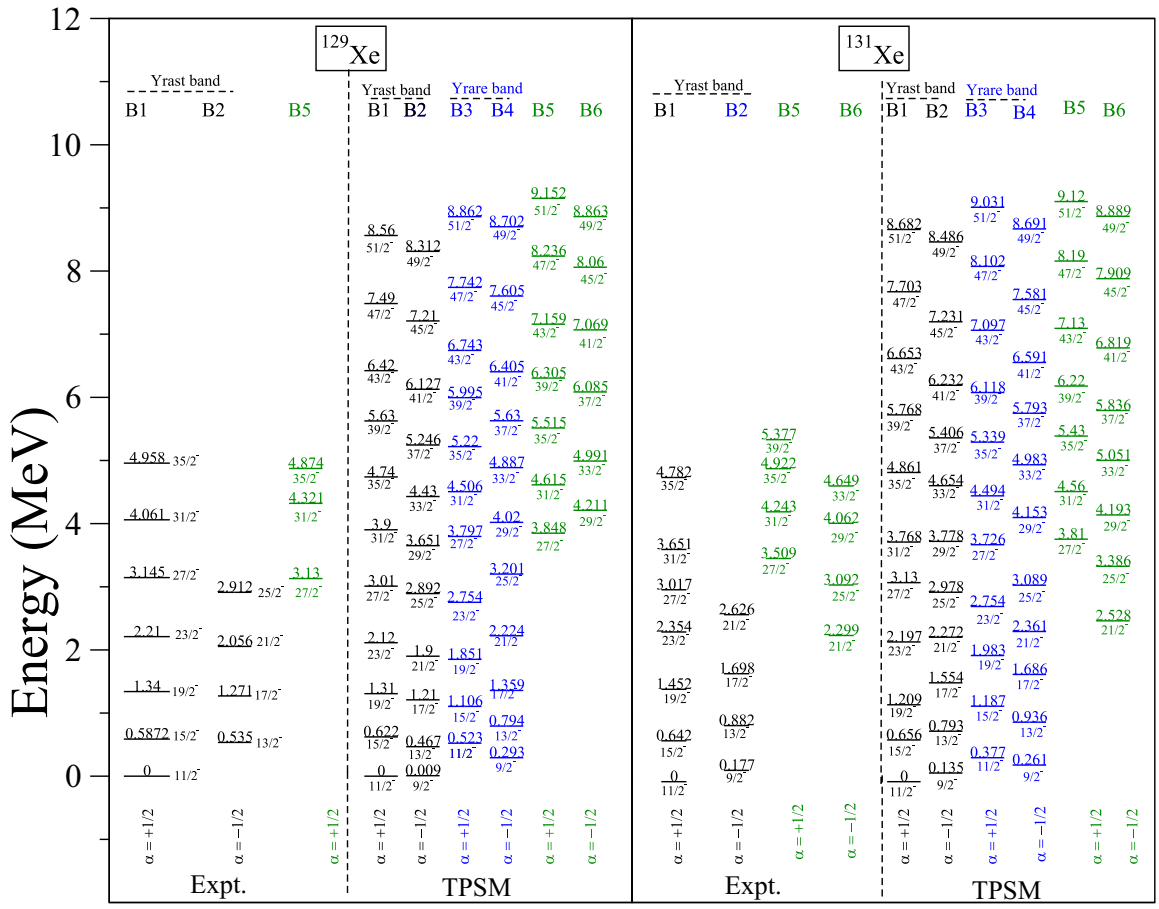

FIG. 7. TPSM energies for the lowest bands after configuration mixing are plotted along with the available experimental data for ^{129,131}Xe isotopes. Data were taken from [51–53].

to elucidate the intrinsic structures, where these bands have already been identified. For other nuclei, the predicted band structures will provide some guidance for future experimental investigations.

For ^{117}Xe, the yrast band is known up to $I = 43/2$ for the favored signature ($\alpha = 1/2$) and up to $I = 33/2$ for the unfavored signature ($\alpha = -1/2$). The calculated TPSM energies, shown in Fig. 4, are noted to be in good agreement with the known energies. The deviation between experimental and the calculated energy for the highest observed spin state is about 0.15 MeV. In Fig. 4, the TPSM energies are also given for the yrare and the second excited band. In some Xecisotopes, excited band structures have been observed and we hope that in future experimental studies excited structures will also be identified for ^{117}Xe. Figure 4 also compares the known experimental bands with the TPSM calculated energies for ^{119}Xe. For this system, apart from the yrast band that is observed up to $I = 43/2$, yrare band is also known up to $I = 29/2$. It is evident from the figure that TPSM calculations reproduce the experimental energies fairly well. The unfavored branch of the γ band is lower in energy as compared to the favoured branch for low spin, and then at higher spin the situation is reversed. The signature splitting of the γ bands will be discussed in detail later.

The calculated band structures for ^{121}Xe and ^{123}Xe are compared with the known energies in Fig. 5. The yrare band up to $I = 29/2$ is observed in ^{121}Xe, and in ^{123}Xe apart from the yrare band one more excited band is known. The band structures for the isotopes of ^{125}Xe and ^{127}Xe are compared in Fig. 6, and it is noted that agreement between the TPSM and the known experimental energies is quite reasonable. For both the isotopes, apart from the yrare band, one more excited band is known with the bandshead at $I = 27/2$. The results for ^{129}Xe and ^{131}Xe are compared in Fig. 7, and again the TPSM energies are in good agreement with the known energies. For both these isotopes, excited bands have been observed, which are quite high in energy and appear to be based on three-quasiparticle configuration. In the following, we shall examine the intrinsic structures of the bands, presented in Figs. 4–7, through the analysis of the wave functions.

The wave function amplitudes of the yrast, yrare, and the second excited bands are displayed in Figs. 8–10, respectively for the eight studied isotopes. The yrast band at low-spin has the dominant contribution from the projected one-quasineutron configuration with $K = 3/2$. At high-spin, the three-quasiparticle state which crosses the ground-state band becomes dominant. For ^{117}Xe, the one-neutron coupled to two-proton configuration crosses and, therefore, the first band crossing is due to the alignment of protons. For the

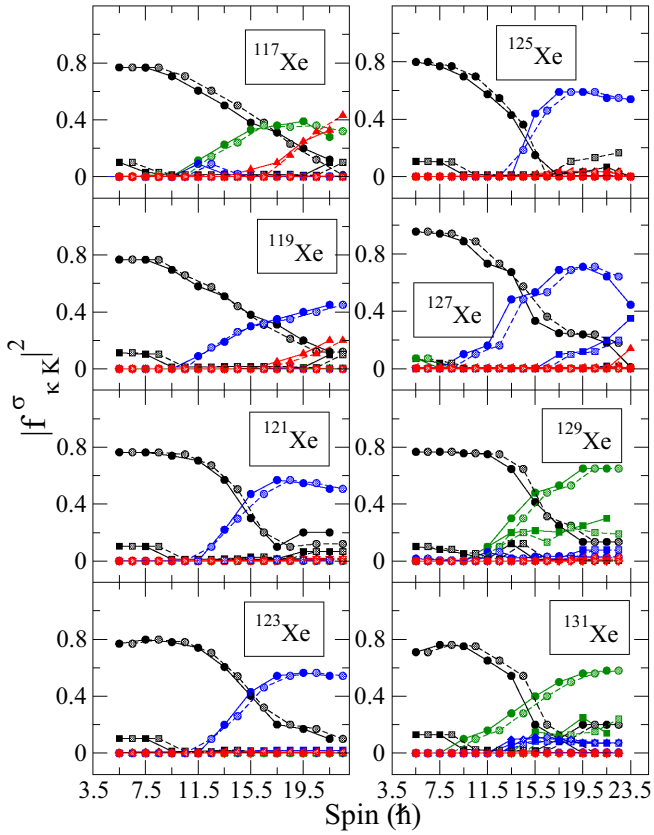

FIG. 8. Amplitudes of various projected K configurations in the wave functions of the yrast band after diagonalization for $^{117-131}$Xe isotopes. The curves are labeled as in Fig. 1. It needs to be clarified that the projected basis states are not orthogonal, and the amplitudes displayed are not probabilities in the true sense. However, qualitative features of the wave-function amplitudes will not change after the orthogonalization is performed as has been done in some studies [54,55].

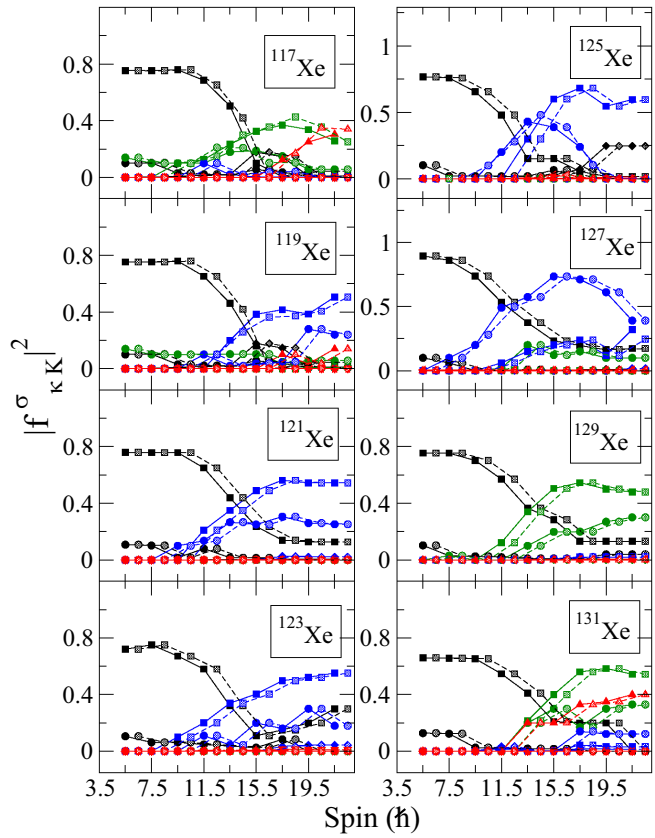

FIG. 9. Amplitudes of various projected K configurations in the wave functions of the yrare band after diagonalization for $^{117-131}$Xe isotopes. The curves are labeled as in Fig. 1.

isotopes from ^{119}Xe to ^{127}Xe, it is three-quasineutron configuration that crosses the ground-state band and the first crossing for these isotopes is due to alignment of neutrons. For the two heavier isotopes of ^{129}Xe and ^{131}Xe, the crossing is due to protons as for ^{117}Xe. It is also noted from Fig. 8 that the five-quasiparticle state becomes important at high-spin, in particular, for ^{117}Xe.

The amplitudes for the yrare band, Fig. 9, which is a γ band in the low-spin region also depicts a crossing phenomenon similar to that of the yrast band. For the yrast band, the band crossing is due to the alignment of three quasiparticles and in the case of the yrare band, it is the γ band built on this parent three-quasiparticle state. What is interesting is that angular-momentum at the crossing point is similar for the yrast and the γ band. Therefore, γ band tracks the yrast band for the studied odd-neutron Xe-isotopes as has been observed for the even-even ^{156}Dy nucleus [13].

In Fig. 10, the wave function amplitudes for the second excited band are shown for the eight Xe-isotopes. These bands have been observed for some of the studied isotopes. In general, it is noted from the figure that the wave function of the excited band have mixed intrinsic compositions due to high density of states at higher excitation energies. For ^{117}Xe, ^{119}Xe, ^{121}Xe, ^{123}Xe, ^{125}Xe and ^{127}Xe, low-spin states have dominant three-neutron configuration, and at high-spin the five-quasiparticle state becomes important. One-neutron coupled to two-proton configuration is dominant for ^{129}Xe and ^{131}Xe isotopes.

It is expected that in future experimental studies many three-quasiparticle band structures will be identified at high spin. To provide some guidance to these studies, we have investigated the angular momentum dependence of the lowest few three-quasiparticle bands that become favored at high spin. The bandheads of these bands are depicted in Fig. 11 with reference to the yrast state for each angular momentum. These energies have been calculated after diagonalization of the shell model Hamiltonian and have mixing from various quasiparticle states. The dominant component for each band head is indicated in the legend of Fig. 11. It is quite evident from the figure that, for low I, these states are quite high in excitation energy, but become favored in the high-spin region. In particular, it is noted that the γ band built on the three-quasiparticle states come close to the yrast line at high spin.

The observation of anomalous signature splitting of negative parity bands in odd-A Xe isotopes has attracted considerable attention in recent years [47,85]. There are four negative parity rotational bands, viz., favored and unfavored

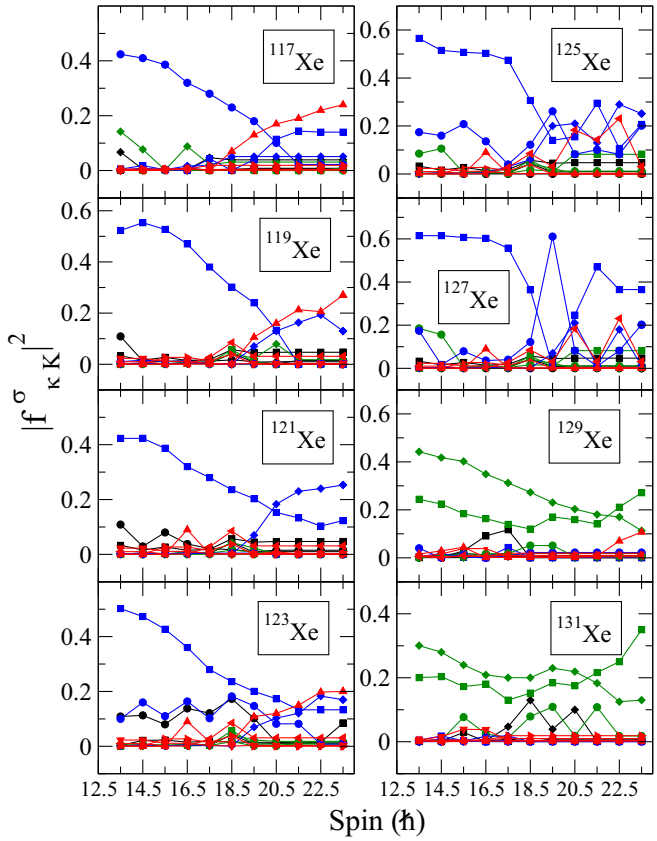

FIG. 10. Amplitudes of various projected K configurations in the wave functions of the second excited band after diagonalization for $^{117-131}$Xe isotopes. The curves are labeled as in Fig. 1.

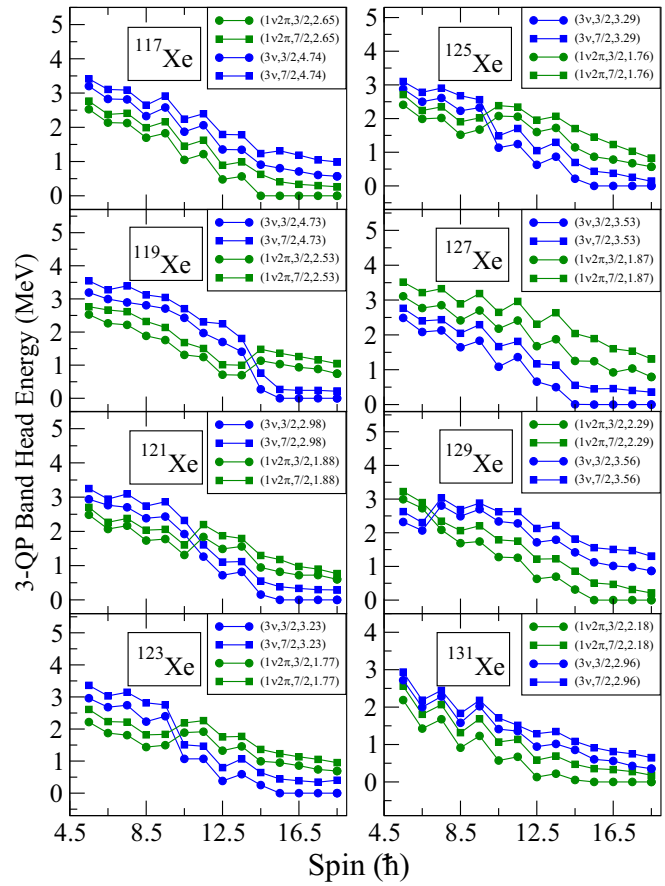

FIG. 11. Lowest few calculated three-quasiparticle bandhead energies after configuration mixing for odd-neutron $^{117-131}$Xe isotopes. The bandhead energies are plotted with respect to the lowest state at each angular momentum.

signature partners ($\alpha = \pm 1/2$) of the yrast and yrare bands, based on the $\nu h_{11/2}$ orbital that are reported systematically in odd-A Xe isotopes. The yrast band was reported in $^{117-131}$Xe with large signature splitting. The origin of this band is explained in terms of the coupling of a quasineutron in the $h_{11/2}$ orbital to the ground state configuration of the core (i.e., $\nu h_{11/2} \otimes 0^+_1|_{^{\text{even}}\text{Xe}}$). However, the observed large signature splitting in this band is quite unexpected for a band associated with high-Ω quasiparticles ($\Omega \geqslant \frac{3}{2}$). Theoretical calculations predict that the signature splitting of yrast negative parity bands is very sensitive to the γ deformation [86]. For instance, the observed $S(I)$ in the case of ^{125}Xe ($[523]\frac{7}{2}$) is reproduced well with $\gamma \approx 24^\circ$ [87]. However, the $S(I)$ is found to be normal in the case of positive parity bands, in spite of having similar γ deformation [88]. In contrast to the yrast bands, the yrare bands, which are thought to originate from the coupling of an $h_{11/2}$ neutron with the γ vibration of the core (i.e., $\nu h_{11/2} \otimes 2^+_2|_{^{\text{even}}\text{Xe}}$), in $^{119-125}$Xe were reported with a low, fairly constant and inverted signature splitting [85]. But, the $S(I)$ of the quasi-γ bands in $^{\text{even}}$Xe isotopes are not inverted and also vary with the mass number [89]. Therefore, such a simple coupling scheme is not adequate enough to explain the origin of the yrare bands.

To shed light on the observation of signature inversion in some odd-mass Xe isotopes, we have evaluated the signature splitting, $S(I)$, of the yrast and the γ bands using the TPSM energies. The calculated signature splitting and the corresponding experimental values for the two bands are displayed in Figs. 12 and 13. It is evident from Fig. 12 that the calculations reproduce the experimental signature splitting for the yrast band quite well, and this is a validation that γ deformation values employed in the TPSM model are reasonable. For the isotopes of ^{119}Xe and ^{125}Xe, the yrare band is known up to high spin and it is observed that the favored signature lies higher in energy than the unfavored one for the low-spin states, and then around $I = 12$ signature inversion is noted. It is evident from Fig. 13 that signature inversion is well reproduced by the TPSM calculations, and is readily understood as due to the crossing of the three-quasiparticle band with the γ band as is seen from the band diagrams, Figs. 1–3. The two crossing configurations have opposite signature phase and gives rise to signature inversion. For ^{119}Xe, the TPSM calculated $S(I)$ depicts another signature inversion at about $I = 17$ and is due to the interaction with other quasiparticle configurations.

It is noted that the three-quasiparticle band crosses the γ bands in all the Xe isotopes and it is, therefore, expected that for all the studied nuclei the γ band will depict a change in the signature phase. For ^{121}Xe and ^{123}Xe, the observed favored

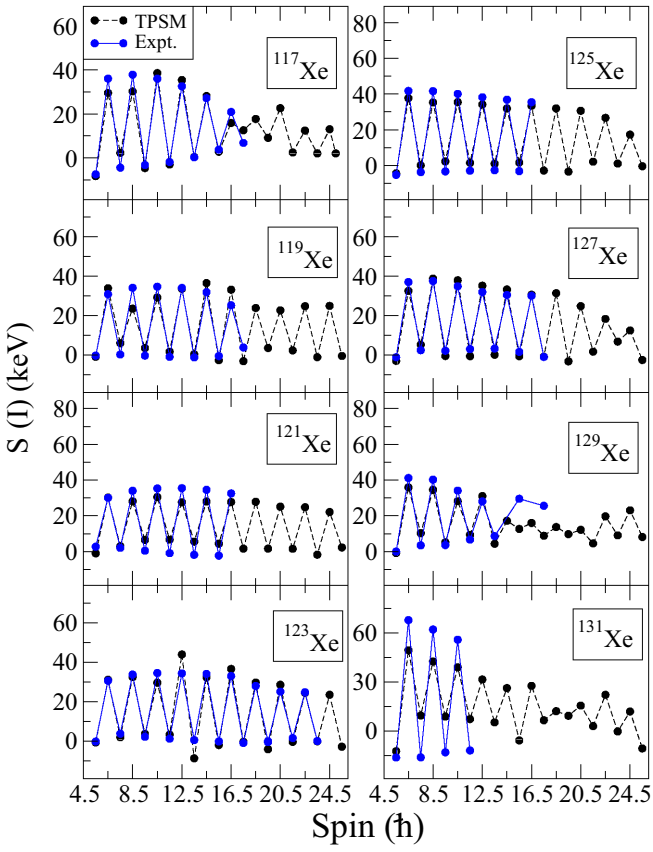

FIG. 12. Plots of the signature splitting of the negative-parity yrast-bands in $^{117-131}$Xe nuclei with $S(I) = [E(I) - E(I-1)]/2I$.

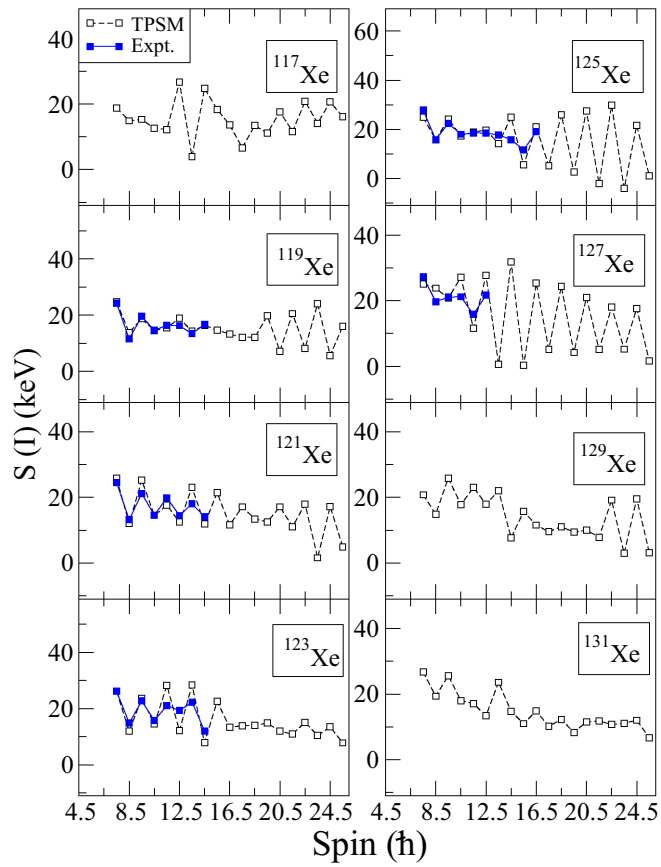

FIG. 13. Plots of the signature splitting of the negative-parity yrare-bands in $^{117-131}$Xe nuclei with $S(I) = [E(I) - E(I-1)]/2I$.

signature again lies at a higher energy than the unfavored one, but no inversion is noted. The inversion is seen at a higher angular momentum in the TPSM calculated $S(I)$. For ^{127}Xe, the inversion is observed at a slightly lower angular momentum and is again well reproduced by the TPSM calculations. For the three isotopes of ^{117}Xe, ^{129}Xe, and ^{131}Xe, yrare bands have not been observed, but the theoretical calculations predict a similar behavior of $S(I)$ as for other isotopes. The yrast band $S(I)$, shown in Fig. 12, does not depict any signature inversion at the crossing point as the phases of the signature splitting of both the bands is the same, although some modification in the signature splitting is noted after the band crossing since the two bands have different $S(I)$.

We shall now turn to the discussion of the band crossing features for the studied Xe isotopes. It has been demonstrated in several studies that the nature of the first band crossing changes with the shell filling [76,90,91]. In order to investigate the detailed features of crossing phenomena, we have calculated the following quantities: aligned angular momentum (i_x) and dynamic moment of inertia ($J^{(2)}$). These quantities are displayed in Figs. 14–17 for the yrast and the yrare bands. In the captions of Figs. 14 Fig. 16, the expressions and the parameters used to evaluate i_x and $J^{(2)}$ are provided. For the yrast bands of ^{119}Xe, ^{123}Xe, ^{129}Xe, and ^{131}Xe, i_x in Fig. 14 depict back-bends, indicating that the crossing between the bands is weak. For the other isotopes, i_x depict up-bends, which suggests that the interaction between the two bands is large. For ^{125}Xe, back-bend is noted at a higher rotational frequency. The TPSM calculated i_x for the yrare band, displayed in Fig. 15, depict back-bends in all the cases. The experimental values are known only in the low-spin regime and TPSM calculations reasonably reproduce these values. The dynamic moment of inertia values, compared in Figs. 16 and 17 for the yrast and the yrare bands, show a reasonable agreement between the TPSM calculated numbers and those deduced from the experimental data. TPSM calculated $J^{(2)}$ for the yrare band depicts large structural changes for all the studied isotopes as this band interacts with many other bands.

We have also studied the transition quadruple moment, Q_t, along the yrast and yrare bands since the quasiparticle alignments are expected to give rise to deformation changes. The calculated Q_t for the two bands are depicted in Fig. 18 and it is noted that, for all the isotopes, Q_t drops in the band crossing region. This drop is expected since in this region the wave function is a mixture of ground and the aligning configurations. Further, it is noted that yrast and yrare bands have similar behavior, and this is easily understood since both the bands originate from the same intrinsic configuration and also have similar band crossing features. The difference in the magnitudes of Q_t for the two bands can be mainly attributed to the different K composition in the two bands: the yrast

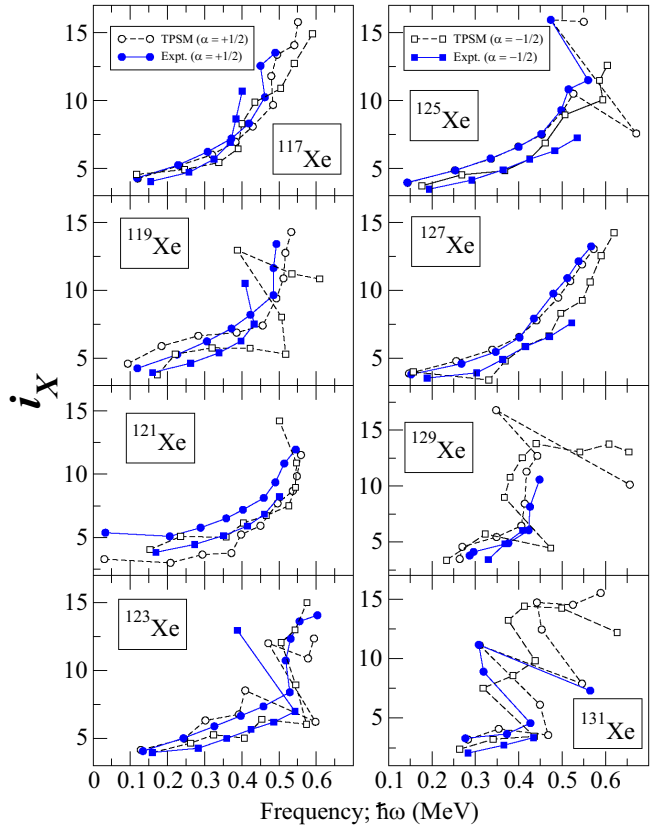

FIG. 14. Comparison of the aligned angular momenta, $i_x = I_x(\omega) - I_{x,\mathrm{ref}}(\omega)$, where $\hbar\omega = \frac{E_\gamma}{I_x^i(\omega) - I_x^f(\omega)}$, $I_x(\omega) = \sqrt{I(I+1) - K^2}$, and $I_{x,\mathrm{ref}}(\omega) = \omega(J_0 + \omega^2 J_1)$. The reference band Harris parameters used are $J_0 = 23$ and $J_1 = 90$, obtained from the measured energy levels as well as those calculated from the TPSM results, for $^{117-131}$Xe nuclei.

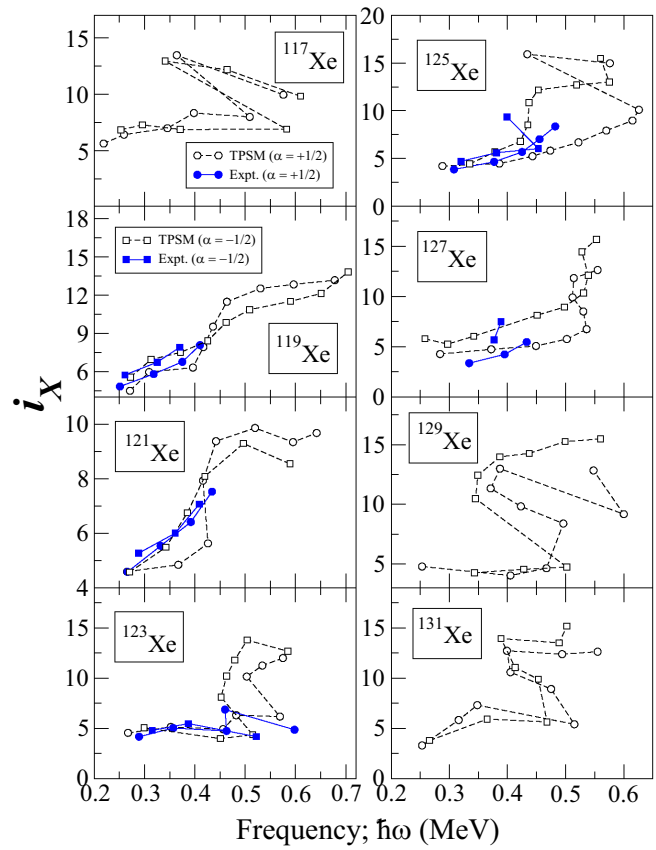

FIG. 15. Comparison of the aligned angular momenta for the yrare band obtained from the measured energy levels as well as those calculated from the TPSM results, for $^{117-131}$Xe nuclei.

band is dominated by $K = 3/2$ whereas the yrare band has the $K = 7/2$ predominant component.

IV. SUMMARY AND CONCLUSIONS

In the present work, the triaxial projected shell model approach has been extended to include three-neutron and five-quasiparticle configurations for odd-neutron systems. This generalization has made it feasible to investigate the intrinsic structures of the observed excited bands in odd-neutron systems. For odd-mass Xe isotopes, several excited band structures have been observed, and the configurations of these bands have been discussed. As the protons and neutrons occupy the same configuration space, the interplay between them plays a crucial role to determine the structures of the observed bands. In the earlier version of the TPSM approach, the basis space for odd-neutron systems comprised one-neutron and one-neutron coupled to two-proton states, and it was not possible to study the interplay between neutron and proton aligned configuration. It is known from the CSM analysis [76] that the nature of the band crossing changes from proton to neutron with the $1h_{11/2}$ shell filling. It has been elucidated using the extended model space that band crossing for ^{117}Xe is due to the alignment of protons, and for ^{119}Xe to ^{127}Xe it is due to the alignment of neutrons. For the two isotopes ^{129}Xe and ^{131}Xe, it is again due to the alignment of protons.

Further, it has been demonstrated that the excited bands observed in some odd-neutron Xe isotopes are actually γ bands based on three-quasiparticle configurations. It has been discussed in several TPSM studies that γ bands are built on each quasiparticle state as for the ground-state band. For even-even systems, several s bands have been identified, and it has been observed in many cases that g factors have similar values for the bandhead 10^+ states [82]. The similar nature of the g factors was quite surprising as normally one expects different g factors for proton and neutron aligning configurations. In this region, both neutrons and protons tend to align almost simultaneously as the two Fermi surfaces are in close vicinity. It is then expected that one s band should have neutron character, and the other to have the proton structure. The observation of similar g factors was puzzling as they should be different, corresponding to protons and neutrons. It was clarified using the TPSM approach that the two observed s-bands are actually a two-particle aligned configuration and the γ band based on this aligned state [92]. Since the two bands have the same intrinsic structure it is expected that g factors of the two s bands should have similar values. It was shown for ^{134}Ce that the two bands have negative g factors i.e., neutron character, and for ^{136}Nd it was demonstrated that they

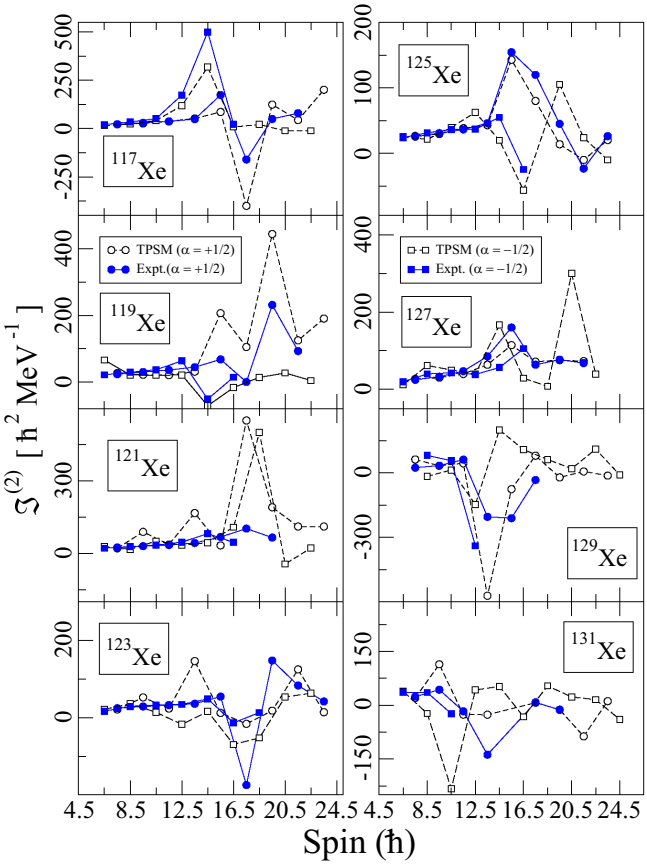

FIG. 16. Comparison between experimental and calculated dynamic moments of inertia, $J^{(2)} = \frac{4}{E_\gamma(I)-E_\gamma(I-2)}$, of the yrast band for $^{117-131}$Xe isotopes.

have proton character as the two lowest aligned bands have positive g factor [92].

For odd-mass systems, we also expect a similar band crossing phenomenon in this region. It has been shown in the present work that the three-quasiparticle band crosses the one-quasiparticle ground-state band and leads to the standard band crossing phenomenon observed along the yrast line. The interesting inference from the present work is that the normal γ band, which is the first excited band, is also crossed by a γ band based on the three-quasiparticle configuration that crosses the ground-state band. Therefore, the γ band tracks the ground-state band with analogous band crossing occurring in the two bands [13]. It has been further observed that some γ bands in Xe isotopes depict signature inversion at high spin, and it is now quite evident from the present investigation that this inversion is directly related to the occurrence of the band crossing along the γ band. The three-quasiparticle band that crosses the ground-state band at high spin first crosses the γ band at a lower spin and gives rise to signature inversion as the two bands have opposite phase of the signature splitting.

We have also provided excitation energies of the three-quasiparticle configurations, which become favored at high spin. Some of these band structures have already been observed in a few isotopes, and we hope that in future experimental work many more excited bands will be identified.

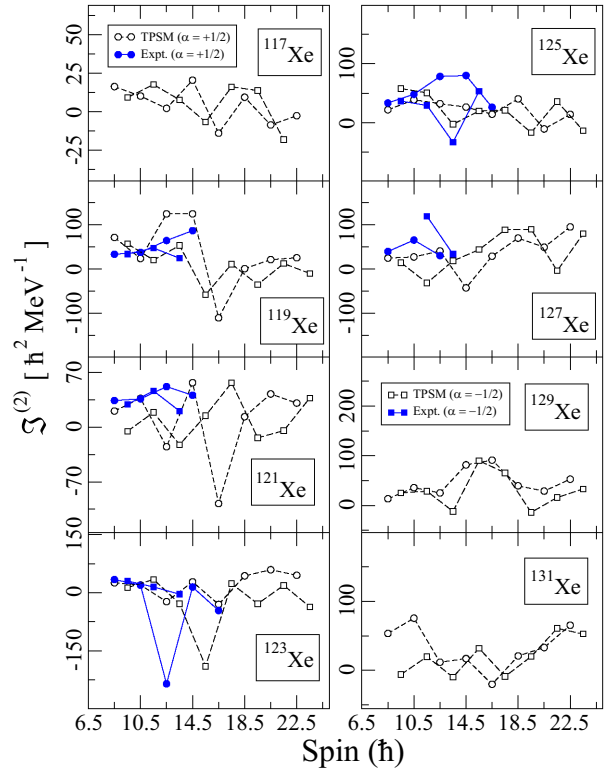

FIG. 17. Comparison between experimental and calculated dynamic moments of inertia of the yrare-band for $^{117-131}$Xe isotopes.

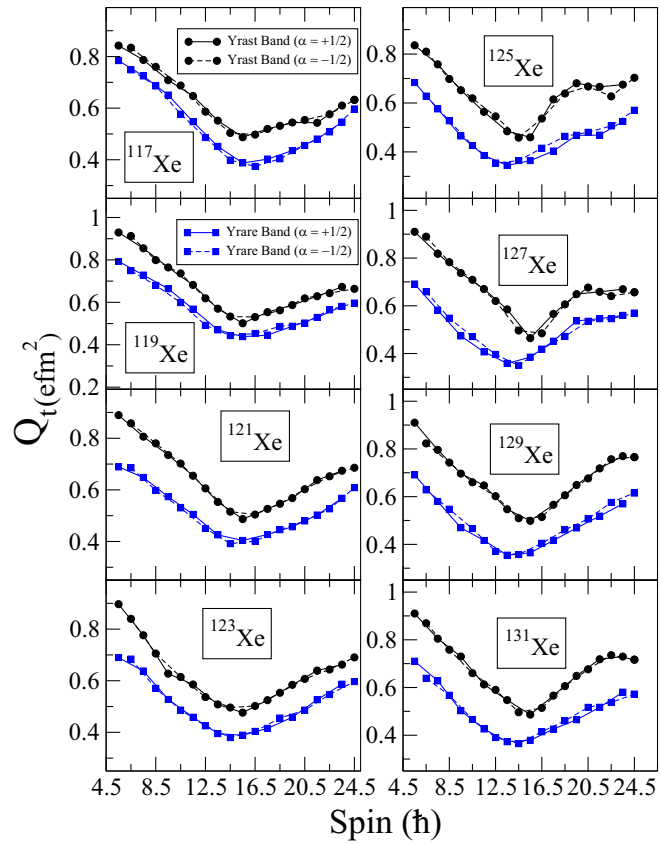

FIG. 18. Calculated transition quadrupole moments, Q_t (e fm^2), for yrast and yrare bands in $^{117-131}$Xe isotopes.

It will be interesting to measure the g factors of these excited bands at high spin as some of these bands are γ bands based on three-quasiparticle configurations and will have similar g factor as that of the parent band. Further, the transition quadrupole moment has been studied, and it has been demonstrated that both yrast and yrare bands have similar behavior as a function of spin.

ACKNOWLEDGMENTS

The authors would like to acknowledge the Science and Engineering Research Board (SERB), Department of Science and Technology (Govt. of India) for providing financial assistance under Project No. CRG/2019/004960 to carry out a part of the present research work.

[1] I-Yang Lee, Prog. Part. Nucl. Phys. **28**, 473 (1992).
[2] W. Korten, A. Atac, D. Beaumel, P. Bednarczyk, M. A. Bentley, G. Benzoni, A. Boston, A. Bracco, J. Cederkäll, B. Cederwall *et al.*, Eur. Phys. J. A **56**, 137 (2020).
[3] F. Beck, Prog. Part. Nucl. Phys. **28**, 443 (1992).
[4] S. Nag, A. K. Singh, A. N. Wilson, J. Rogers, H. Hübel, A. Bürger, S. Chmel, I. Ragnarsson, G. Sletten, B. Herskind *et al.*, Phys. Rev. C **85**, 014310 (2012).
[5] S. Nag, A. K. Singh, I. Ragnarsson, H. Hübel, A. Al-Khatib, P. Bringel, C. Engelhardt, A. Neußer-Neffgen, G. B. Hagemann, B. Herskind *et al.*, Phys. Rev. C **88**, 044335 (2013).
[6] P. Singh, A. K. Singh, A. N. Wilson, J. Rogers, H. Hübel, A. Bürger, S. Chmel, I. Ragnarsson, G. Sletten, B. Herskind *et al.*, Phys. Rev. C **85**, 034319 (2012).
[7] P. Singh, S. Nag, A. K. Singh, I. Ragnarsson, H. Hübel, A. Al-Khatib, P. Bringel, C. Engelhardt, A. Neußer-Neffgen, G. B. Hagemann *et al.*, Phys. Rev. C **84**, 024316 (2011).
[8] A. Basu, A. K. Singh, I. Ragnarsson, B. G. Carlsson, A. Kardan, G. B. Hagemann, G. Sletten, B. Herskind, H. Hübel, S. Chmel *et al.*, Phys. Rev. C **103**, 014301 (2021).
[9] S. Nag, A. K. Singh, G. B. Hagemann, G. Sletten, B. Herskind, T. Døssing, I. Ragnarsson, H. Hübel, A. Bürger, S. Chmel *et al.*, Phys. Rev. C **94**, 034307 (2016).
[10] A. Al-Khatib, G. B. Hagemann, G. Sletten, A. K. Singh, H. Amro, G. Benzoni, A. Bracco, P. Bringel, F. Camera, M. P. Carpenter *et al.*, Phys. Rev. C **83**, 024306 (2011).
[11] C. Rønn Hansen, G. Sletten, G. B. Hagemann, B. Herskind, D. R. Jensen, P. Bringel, C. Engelhardt, H. Hübel, A. Neußer-Neffgen, A. K. Singh *et al.*, Phys. Rev. C **76**, 034311 (2007).
[12] K. K. Zheng, C. M. Petrache, Z. H. Zhang, A. Astier, B. F. Lv, P. T. Greenlees, T. Grahn, R. Julin, S. Juutinen, M. Luoma *et al.*, Phys. Rev. C **104**, 044305 (2021).
[13] S. N. T. Majola, D. J. Hartley, L. L. Riedinger, J. F. Sharpey-Schafer, J. M. Allmond, C. Beausang, M. P. Carpenter, C. J. Chiara, N. Cooper, D. Curien *et al.*, Phys. Rev. C **91**, 034330 (2015).
[14] D. G. Roux, W. C. Ma, G. B. Hagemann, H. Amro, D. R. Elema, P. Fallon, A. Görgen, B. Herskind, H. Hübel, Y. Li *et al.*, Phys. Rev. C **92**, 064313 (2015).
[15] J. N. Wilson, S. J. Asztalos, R. A. Austin, B. Busse, R. M. Clark, M. A. Deleplanque, R. M. Diamond, P. Fallon, S. Flibotte, G. Gervais *et al.*, Phys. Rev. C **56**, 2502 (1997).
[16] D. Negi, S. K. Tandel, P. Chauhan, P. Chowdhury, R. V. F. Janssens, M. P. Carpenter, T. L. Khoo, F. G. Kondev, T. Lauritsen, C. J. Lister *et al.*, Phys. Rev. C **100**, 014329 (2019).
[17] G. Hackman, R. Krücken, R. V. F. Janssens, M. A. Deleplanque, M. P. Carpenter, D. Ackermann, I. Ahmad, H. Amro, S. Asztalos, D. J. Blumenthal *et al.*, Phys. Rev. C **55**, 148 (1997).
[18] M. S. Johnson, J. A. Cizewski, M. B. Smith, J. S. Thomas, J. A. Becker, L. A. Bernstein, A. Schiller, D. P. McNabb, P. Fallon, and A. O. Macchiavelli, Phys. Rev. C **71**, 024317 (2005).
[19] R. Bengtsson and S. Frauendorf, Nucl. Phys. A **327**, 139 (1979).
[20] R. Bengtsson and S. Frauendorf, Nucl. Phys. A **314**, 27 (1979).
[21] J. Dudek, Z. Szymański, and T. Werner, Phys. Rev. C **23**, 920 (1981).
[22] P. Ring and P. Schuck, *The Nuclear Many-Body Problem* (Springer, Berlin, 1980).
[23] T. Otsuka, A. Gade, O. Sorlin, T. Suzuki, and Y. Utsuno, Rev. Mod. Phys. **92**, 015002 (2020).
[24] K. Higashiyama and N. Yoshinaga, Phys. Rev. C **88**, 034315 (2013).
[25] L. Y. Jia, H. Zhang, and Y. M. Zhao, Phys. Rev. C **75**, 034307 (2007).
[26] M. Queiser, A. Vogt, M. Seidlitz, P. Reiter, T. Togashi, N. Shimizu, Y. Utsuno, T. Otsuka, M. Honma, P. Petkov *et al.*, Phys. Rev. C **96**, 044313 (2017).
[27] M. S. R. Laskar, S. Saha, R. Palit, S. N. Mishra, N. Shimizu, Y. Utsuno, E. Ideguchi, Z. Naik, F. S. Babra, S. Biswas *et al.*, Phys. Rev. C **99**, 014308 (2019).
[28] C. Kremer, S. Aslanidou, S. Bassauer, M. Hilcker, A. Krugmann, P. von Neumann-Cosel, T. Otsuka, N. Pietralla, V. Y. Ponomarev, N. Shimizu *et al.*, Phys. Rev. Lett. **117**, 172503 (2016).
[29] E. Teruya, N. Yoshinaga, K. Higashiyama, and A. Odahara, Phys. Rev. C **92**, 034320 (2015).
[30] N. Yoshinaga and K. Higashiyama, Phys. Rev. C **69**, 054309 (2004).
[31] J. Erler, N. Birge, M. Kortelainen, W. Nazarewicz, E. Olsen, A. M. Perhac, and M. Stoitsov, Nature (London) **486**, 509 (2012).
[32] N. Schunck, ed., *Energy Density Functional Methods for Atomic Nuclei*, 2053-2563 (IOP, Bristol, 2019).
[33] R. J. Furnstahl, Eur. Phys. J. A **56**, 85 (2020).
[34] S. Goriely, S. Hilaire, M. Girod, and S. Péru, Phys. Rev. Lett. **102**, 242501 (2009).
[35] L. M. Robledo, T. R. Rodríguez, and R. R. Rodríguez-Guzmán, J. Phys. G: Nucl. Part. Phys. **46**, 013001 (2019).
[36] P. Ring, Prog. Part. Nucl. Phys. **37**, 193 (1996).
[37] J. Dobaczewski, M. V. Stoitsov, W. Nazarewicz, and P.-G. Reinhard, Phys. Rev. C **76**, 054315 (2007).
[38] T. Duguet, M. Bender, K. Bennaceur, D. Lacroix, and T. Lesinski, Phys. Rev. C **79**, 044320 (2009).
[39] J. A. Sheikh, J. Dobaczewski, P. Ring, L. M. Robledo, and C. Yannouleas, J. Phys. G: Nucl. Part. Phys. **48**, 123001 (2021).
[40] M. Bender, P.-H. Heenen, and P.-G. Reinhard, Rev. Mod. Phys. **75**, 121 (2003).
[41] Y. Alhassid, G. F. Bertsch, L. Fang, and B. Sabbey, Phys. Rev. C **74**, 034301 (2006).
[42] R. Rodríguez-Guzmán, Y. Alhassid, and G. F. Bertsch, Phys. Rev. C **77**, 064308 (2008).
[43] K. Nomura, T. Nikšić, T. Otsuka, N. Shimizu, and D. Vretenar, Phys. Rev. C **84**, 014302 (2011).

[44] K. Nomura, D. Vretenar, Z. P. Li, and J. Xiang, Phys. Rev. C **104**, 024323 (2021).

[45] K. Nomura, R. Rodríguez-Guzmán, and L. M. Robledo, Phys. Rev. C **104**, 054320 (2021).

[46] Z. Liu, X. Sun, X. Zhou, X. Lei, Y. Guo, Y. Zhang, X. Chen, H. Jin, Y. Luo, S. X. Wen *et al.*, Eur. Phys. J. A **1**, 125 (1998).

[47] C.-B. Moon, T. Komatsubara, Y. Sasaki, T. Jumatsu, K. Yamada, K. Satou, and K. Furuno, Eur. Phys. J. A **14**, 13 (2002).

[48] J. Timár, J. Simpson, E. S. Paul, S. Araddad, C. W. Beausang, M. A. Bentley, M. J. Joyce, and J. F. Sharpey-Schafer, Phys. Scr. **T56**, 325 (1995).

[49] S. Chakraborty, H. P. Sharma, S. S. Tiwary, C. Majumder, A. K. Gupta, P. Banerjee, S. Ganguly, S. Rai, Pragati, Mayank *et al.*, Phys. Lett. B **811**, 135854 (2020).

[50] S. Chakraborty, H. P. Sharma, S. S. Tiwary, C. Majumder, P. K. Prajapati, S. Rai, P. Popli, M. Singh, S. S. Bhattacharjee, R. P. Singh *et al.*, Braz. J. Phys. **47**, 406 (2017).

[51] Y. Huang, Z. G. Xiao, S. J. Zhu, C. Qi, Q. Xu, W. J. Cheng, H. J. Li, L. M. Lyu, R. S. Wang, W. H. Yan *et al.*, Phys. Rev. C **93**, 064315 (2016).

[52] R. Banik, S. Bhattacharyya, S. Biswas, S. Bhattacharya, G. Mukherjee, S. Rajbanshi, S. Dar, S. Nandi, S. Ali, S. Chatterjee *et al.*, Phys. Rev. C **101**, 044306 (2020).

[53] S. Chakraborty, S. Bhattacharyya, R. Banik, S. Bhattacharya, G. Mukherjee, S. Biswas, S. Rajbanshi, S. Dar, S. Nandi, S. Ali *et al.*, Proc. DAE Symp. Nucl. Phys. **65**, 48 (2021).

[54] F.-Q. Chen and J. L. Egido, Phys. Rev. C **95**, 024307 (2017).

[55] L.-J. Wang, F.-Q. Chen, and Y. Sun, Phys. Lett. B **808**, 135676 (2020).

[56] J. A. Sheikh and K. Hara, Phys. Rev. Lett. **82**, 3968 (1999).

[57] J. A. Sheikh, G. H. Bhat, W. A. Dar, S. Jehangir, and P. A. Ganai, Phys. Scr. **91**, 063015 (2016).

[58] S. Jehangir, G. H. Bhat, J. A. Sheikh, S. Frauendorf, W. Li, R. Palit, and N. Rather, Eur. Phys. J. A **57**, 308 (2021).

[59] J. A. Sheikh, G. H. Bhat, Y. Sun, G. B. Vakil, and R. Palit, Phys. Rev. C **77**, 034313 (2008).

[60] J. A. Sheikh, G. H. Bhat, R. Palit, Z. Naik, and Y. Sun, Nucl. Phys. A **824**, 58 (2009).

[61] J. A. Sheikh, G. H. Bhat, Y. Sun, and R. Palit, Phys. Lett. B **688**, 305 (2010).

[62] J. A. Sheikh, G. H. Bhat, Y.-X. Liu, F.-Q. Chen, and Y. Sun, Phys. Rev. C **84**, 054314 (2011).

[63] G. H. Bhat, J. A. Sheikh, Y. Sun, and U. Garg, Phys. Rev. C **86**, 047307 (2012).

[64] G. H. Bhat, J. A. Sheikh, and R. Palit, Phys. Lett. B **707**, 250 (2012).

[65] J. Marcellino, E. H. Wang, C. J. Zachary, J. H. Hamilton, A. V. Ramayya, G. H. Bhat, J. A. Sheikh, A. C. Dai, W. Y. Liang, F. R. Xu *et al.*, Phys. Rev. C **96**, 034319 (2017).

[66] S. Jehangir, G. H. Bhat, J. A. Sheikh, S. Frauendorf, S. N. T. Majola, P. A. Ganai, and J. F. Sharpey-Schafer, Phys. Rev. C **97**, 014310 (2018).

[67] S. Jehangir, I. Maqbool, G. H. Bhat, J. A. Sheikh, R. Palit, and N. Rather, Eur. Phys. J. A **56**, 197 (2020).

[68] S. Jehangir, G. H. Bhat, N. Rather, J. A. Sheikh, and R. Palit, Phys. Rev. C **104**, 044322 (2021).

[69] L.-J. Wang, F.-Q. Chen, T. Mizusaki, M. Oi, and Y. Sun, Phys. Rev. C **90**, 011303(R) (2014).

[70] L.-J. Wang, Y. Sun, T. Mizusaki, M. Oi, and S. K. Ghorui, Phys. Rev. C **93**, 034322 (2016).

[71] L.-J. Wang, Y. Sun, and S. K. Ghorui, Phys. Rev. C **97**, 044302 (2018).

[72] L.-J. Wang, L. Tan, Z. Li, G. W. Misch, and Y. Sun, Phys. Rev. Lett. **127**, 172702 (2021).

[73] B. Bally, B. Avez, M. Bender, and P.-H. Heenen, Phys. Rev. Lett. **113**, 162501 (2014).

[74] M. Borrajo and J. L. Egido, Phys. Lett. B **764**, 328 (2017).

[75] A. Basu, A. K. Singh, S. Nag, G. B. Hagemann, G. Sletten, B. Herskind, A. N. Wilson, J. Rogers, I. Ragnarsson, H. Hübel *et al.*, Phys. Rev. C **101**, 024309 (2020).

[76] L. Kaya, A. Vogt, P. Reiter, M. Siciliano, B. Birkenbach, A. Blazhev, L. Coraggio, E. Teruya, N. Yoshinaga, K. Higashiyama *et al.*, Phys. Rev. C **98**, 014309 (2018).

[77] K. Kumar and M. Baranger, Nucl. Phys. A **122**, 273 (1968).

[78] M. Dufour and A. P. Zuker, Phys. Rev. C **54**, 1641 (1996).

[79] S. G. Nilsson, C. F. Tsang, A. Sobiczewski, Z. SzymaÅď ski, S. Wycech, C. Gustafson, I.-L. Lamm, P. Möller, and B. Nilsson, Nucl. Phys. A **131**, 1 (1969).

[80] K. Hara and Y. Sun, Int. J. Mod. Phys. E **04**, 637 (1995).

[81] Y. Sun and J. L. Egido, Nucl. Phys. A **580**, 1 (1994).

[82] R. Wyss, A. Granderath, R. Bengtsson, P. von Brentano, A. Dewald, A. Gelberg, A. Gizon, J. Gizon, S. Harissopulos, A. Johnson *et al.*, Nucl. Phys. A **505**, 337 (1989).

[83] R. Wyss, J. Nyberg, A. Johnson, R. Bengtsson, and W. Nazarewicz, Phys. Lett. B **215**, 211 (1988).

[84] A. Zemel, C. Broude, E. Dafni, A. Gelberg, M. B. Goldberg, J. Gerber, G. J. Kumbartzki, and K.-H. Speidel, Nucl. Phys. A **383**, 165 (1982).

[85] C.-B. Moon, C. S. Lee, T. Komatsubara, Y. Sasaki, and K. Furuno, Phys. Rev. C **76**, 067301 (2007).

[86] A. Gelberg, D. Lieberz, P. von Brentano, I. Ragnarsson, P. B. Semmes, and I. Wiedenhöver, Nucl. Phys. A **557**, 439 (1993).

[87] D. Lieberz, A. Gelberg, P. Von Brentano, I. Ragnarsson, and P. B. Semmes, Phys. Lett. B **282**, 7 (1992).

[88] S. Chakraborty, H. P. Sharma, S. S. Tiwary, C. Majumder, P. Banerjee, S. Ganguly, S. Rai, P. Popli, S. Modi, P. Arumugam *et al.*, Eur. Phys. J. A **56**, 50 (2020).

[89] S. Chakraborty, H. P. Sharma, S. S. Tiwary, C. Majumder, P. Banerjee, S. Ganguly, S. Rai, Pragati, Mayank, S. Kumar *et al.*, Nucl. Phys. A **996**, 121687 (2020).

[90] A. Granderath, P. Mantica, R. Bengtsson, R. Wyss, P. von Brentano, A. Gelberg, and F. Seiffert, Nucl. Phys. A **597**, 427 (1996).

[91] A. Ibáñez-Sandoval, M. E. Ortiz, V. Velázquez, A. Galindo-Uribarri, P. O. Hess, and Y. Sun, Phys. Rev. C **83**, 034308 (2011).

[92] S. Jehangir, G. H. Bhat, J. A. Sheikh, R. Palit, and P. A. Ganai, Nucl. Phys. A **968**, 48 (2017).